

# Characterization of the Micromechanical Flying Insect by Optical Position Sensing

E. Steltz, R.J. Wood, S. Avadhanula and R.S. Fearing  
Department of EECS, University of California, Berkeley, CA 94720

{ees132 srinath rjwood ronf} @eecs.berkeley.edu

**Abstract**—In the following work, we develop a characterization method using miniature fiberoptic position sensors for the Micromechanical Flying Insect (MFI)<sup>1</sup>, a centimeter sized micro aerial vehicle being developed at the University of California, Berkeley. Sensing the state of a structure of this scale is challenging due to limited sensor technology and difficulty in constraining the structure. We developed a unique fiberoptic reflection position sensor and associated circuitry that yields a high resolution (approximately 5  $\mu\text{m}$  of linear motion), appropriate scale, and real time method for sensing the state of the MFI. Also included is the development of a clamping technique for the 2 wing, 4 degree of freedom MFI designed to expose actuator surfaces to be sensed while properly grounding the MFI without introducing added compliance or stiffness to the airframe. We include characterization data for a 2 DOF (flapping and rotation for one wing) wing structure, a clamped 4 DOF motor core of the MFI, and one side of an entire 4 DOF MFI.

**Index Terms**—MAV, fiberoptic, optical, characterization, MFI

## I. INTRODUCTION

The Micromechanical Flying Insect (MFI) project at UC Berkeley aims to create a biologically inspired, autonomous, flapping micro aerial vehicle approximately 25 mm in size (wingtip to wingtip). The project started in May 1998 and was inspired by early work by Dickinson et al. [1] who quantified the precise lift mechanisms fruitflies rely upon to fly. Originally the MFI was envisioned to incorporate unimorph piezoelectric bending actuators combined with stainless steel joints and flexures along with an accordion style wing to achieve flight [2]. Advances in all areas of the work, however, have led to the development of novel bimorph piezoelectric actuators along with carbon fiber/polyester links and flexures [3]. Fig. 1 shows the current version of the 4 DOF, 2 wing MFI that weighs approximately 100 mg, without battery or electronics.

The current focus of the project is to realize the proper wing stroke (flapping and rotation) sufficient to achieve the necessary amount of lift. A simple control strategy has been chosen for the MFI (due to actuator limitations) in which the wings will be controlled open loop with the ability to switch between several different wing strokes determined a priori to generate known amounts of forces and torques. To realize open loop control, we must first determine an experimental model of the mechanical plant, at least for certain

<sup>1</sup>This work has been sponsored by ONR MURI N00014-98-1-0671, DARPA, NSF IIS-0083472 and NSF DMI-0115091.

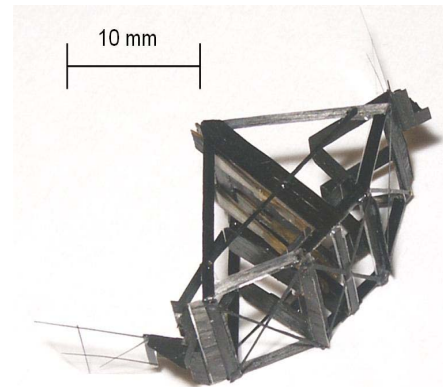


Fig. 1. 4 DOF 2 wing MFI

drive frequencies and amplitudes. The electromechanical plant to be identified consists of bimorph PZT actuators, a fourbar transmission mechanism, a differential mechanism to allow wing rotation and the wing itself. The entire structure appears in Figure 2, showing each link (alpha, beta, and gamma) of the fourbar, and also showing the slider crank and the differential. To realize proper stroke, the wing position itself would ideally be sensed and then controlled, but if the fourbar and differential are considered to have a high serial stiffness (current experimental values are 10000 N/m serial stiffness, 100 N/m parallel stiffness), any part of the fourbar or actuator can be used to infer the position of the wing.

## II. PRIOR MFI SENSING TECHNOLOGIES

Previously, strain gages were mounted on the piezoelectric actuators to measure strain for each actuator. It is known that the strain in an unloaded piezoelectric layer is proportional to the curvature and therefore the tip displacement of the actuator [4], so a strain gage can be an effective position sensor. However, each actuator requires multiple strain gages to eliminate thermal drift; also, with four actuators on each MFI, many wires were required to be attached to the fly during testing. Questions of nonlinearities in the strain on the surface of a loaded PZT actuator and difficult calibration and wiring led to a search for alternative sensing mechanisms. Campolo et al. [5] explored finding strain by using the PZT surface itself as a sensor. A thin section of the piezoelectric surface was electrically separated from the rest of the top conductive

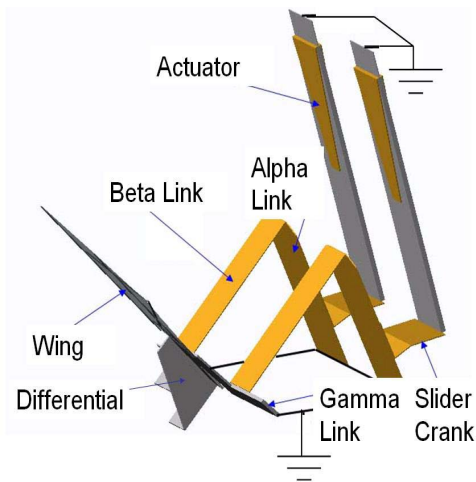


Fig. 2. Wing drive assembly

surface. As the actuator bends, a charge is induced on this isolated surface, and was sensed with a charge amplifier and is proportional to the strain in the actuator, yielding a position measurement. However, this method still required additional wires be attached to the MFI during testing. It also yielded no DC output, and questions again of nonlinearities in the PZT itself (e.g. hysteresis) limits ease of use of this sensor.

A much less invasive, well known optical position sensing technology was therefore employed to track the position of the actuator. Off the shelf Omron infrared reflective sensors (model EE-SF5) were aimed at the back of the actuators and yielded accurate position signals. Using this method to identify the mechanical plant and create a desired stroke, 500  $\mu\text{N}$  of lift was reported for a single wing structure [6].

However, the Omron reflective sensors were very large compared with the MFI itself, and thus could not fit close enough together to track the position of two actuators when they were mounted to the airframe for flight testing. Also, as the actuators were scaled down in size (to 0.5 mm at the tip), the sensors provided very little signal and were not sufficiently accurate for characterization. Capacitive sensors were explored as another non contact method, but sensors of this type which had small enough sensing surfaces needed to be too close to the actuator tip to allow it to move properly. Commercial optical sensors were explored, first the Omron E3X-DA21-N fiber optic amplifier with side-sensing E32-D24 optical fibers. This system had an analog output proportional to the intensity of the light received; however, it was much too slow (a pole located at around 30 Hz). The MTI-2000 Fotonic Sensor was also explored, but was cost prohibitive (\$25,000 for four sensing channels). Also, no side-sensing probes for this system are currently available. We therefore designed our own fiberoptic reflective position sensor system inspired by the Omron system tested here to fit size, accuracy, and bandwidth needs.

### III. FIBEROPTIC POSITION SENSING

Using fiberoptics to transport light to and from the reflecting surface like in the tested Omron system was advantageous in many ways (size constraints, elimination of electromagnetic interference, etc.). Therefore, the same side-sensing fiberoptics (Figure 3) as used with the Omron fiberoptic amplifier were used in the custom system. These PMMA (polymethyl methacrylate) sensors measure 2 mm in diameter at the sensor tip, and transmit red light most efficiently (and therefore red light was used for reflection). Acceptable signals are received from these tips if they are placed between 0.5 mm and 10 mm away from the sensing surface.

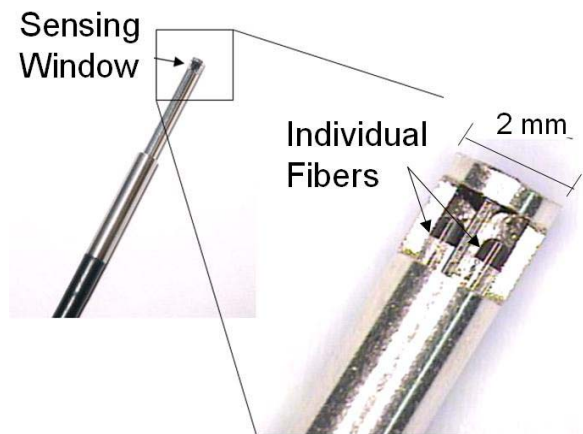


Fig. 3. Omron E32-D24 side sending fiberoptic sensor head

It was realized that simply shining an LED through the fiberoptic and receiving the reflected light into a phototransistor would be difficult due to the attenuation when entering or exiting the fibers. Also, any ambient light could easily combine with the reflected light from the sensing surface and introduce a frequency other than the desired actuator movement frequency.

To solve the problem of attenuation of the fibers, fiberoptic couplers (Industrial Fiberoptics IF-E99 (LED) and IF-D92 (phototransistor)) containing microlenses were used for both the LED and the phototransistor to maximize light transmission as a substitute for the built-in connectors of the Omron fiberoptic amplifier. To solve the ambient light problem, the LED was flashed at a 20 kHz carrier frequency. Once this light was reflected off a much slower moving actuator, the received phototransistor signal is an amplitude modulated waveform. Standard analog circuitry (such as a bandpass filter, absolute value circuits, and low pass filters) was then used to demodulate the signal and achieve a voltage signal proportional to the position of the actuator. A block diagram of the analog signal processing appears in Fig. 4.

All analog circuitry was designed to minimize any introduced dynamics on the sensed position of the actuator. Minimal phase shift (about 11 degrees at 500 Hz) and negligible amplitude change introduced by the circuitry was experimentally verified, as shown in Figure 5 (the

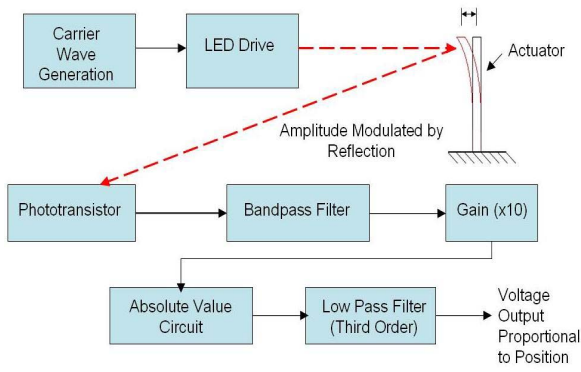


Fig. 4. Block diagram for extracting position from amplitude modulated light

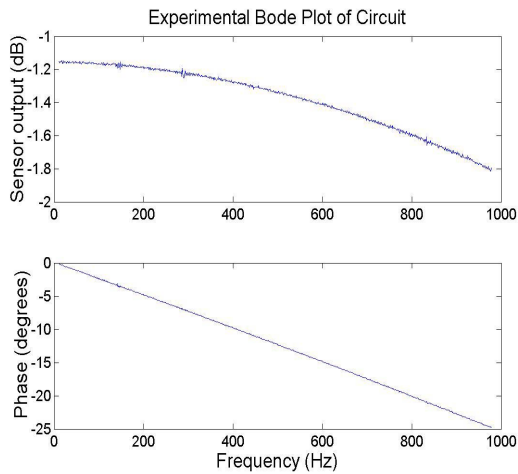


Fig. 5. Analog sensing and demodulation circuit frequency response

experimentally measured transfer function of the analog circuitry). The actuator will be used from DC to about 500 Hz, so as one can see the circuit dynamics are negligible in this range. The real time bandwidth of the sensor system is 3700 Hz, but since circuit dynamics were experimentally identified, offline bandwidth can be as high as 10 kHz.

#### IV. EXPERIMENTAL RESULTS OF OPTICAL POSITION ON 2DOF TEST STAND

A one wing, 2 DOF polyurethane test stand was created and used to verify sensor behavior and to characterize the dynamics of the actuator, fourbar, and wing structure. This stand serves to vibrationally isolate the fourbar and wing structure for testing. A polyurethane actuator mount was constructed, incorporating the actuator itself, actuator wiring, and the newly developed sensor looking directly at the back of the actuator. Two of these mounts (left and right) were then incorporated onto a larger polyurethane base that contained the fourbar, differential, and wing mechanism. The polyurethane actuator base method improves upon the previous 2DOF test stand version using the Omron photomicrosensors because the sensors are now mounted in the same base as the actuators; relative

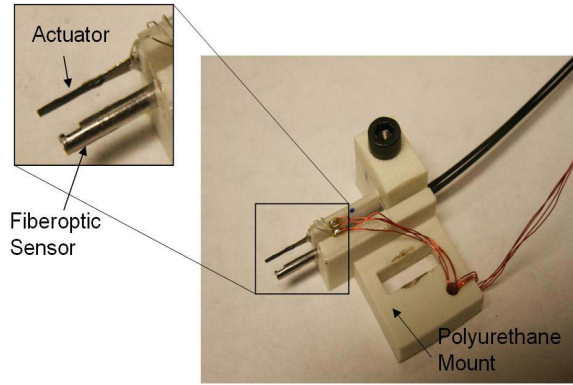


Fig. 6. Actuator and sensor combined test stand mount

movement of the sensor and the actuator can only be due to actuator deflection. The actuator/sensor mount used on the test stand appears in Fig. 6. The actuator tips were also painted with gold metallic paint to reflect the sensor light with greater efficiency, and the sensors were rotated longitudinally until the nominal output was a maximum (which corresponds to highest sensor sensitivity).

While monitoring the fiberoptic sensor output, we measured the displacement of the actuator with a microscope camera and a software edge detection algorithm. A plot of actuator displacement vs sensor output voltage was generated and appears in Fig. 7. The fourbar transmission ratio is 3200 rad/m, and the wing will be flapped through 120 degrees when the MFI is in flight, leading to 655  $\mu\text{m}$  of total actuator motion. The actuator was run at DC over this range to verify monotonicity and linearity of the sensor. It is easily observed that the sensor is approximately linear with respect to deflection. The mean of the line fit error is approximately 0 and the standard deviation is 10.25  $\mu\text{m}$  (coming from either electrical noise, sensor nonlinearity, or software edge detection error). For approximately 25 mV peak to peak of electrical noise or oscillation superimposed on the desired signal, we resolve 3.6  $\mu\text{m}$  of actuator deflection, which corresponds to 0.7 degrees of wing motion.

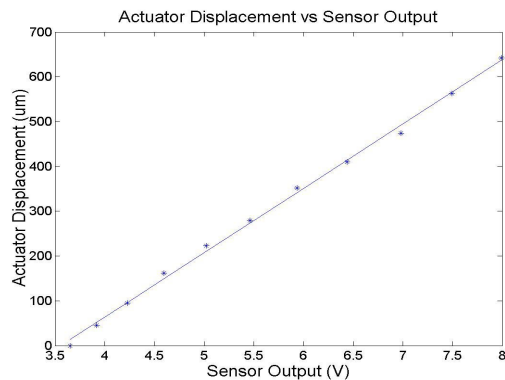


Fig. 7. Sensor linearity with wing angle

Using this test stand and sensor setup on a single wing

2DOF setup, Bode plots were created by driving the two actuators separately. We constructed four total plots; the first actuator was driven and both the position of the driven actuator and the position of the non driven actuator were monitored (coupling through the differential occurs), resulting in two plots. Driving the second actuator also yields two Bode plots. All four Bode plots for a given drive amplitude appear in Figure 8. Approximately second order behavior is observed, and coupling through the differential between the two actuators is significant (as expected)[6].

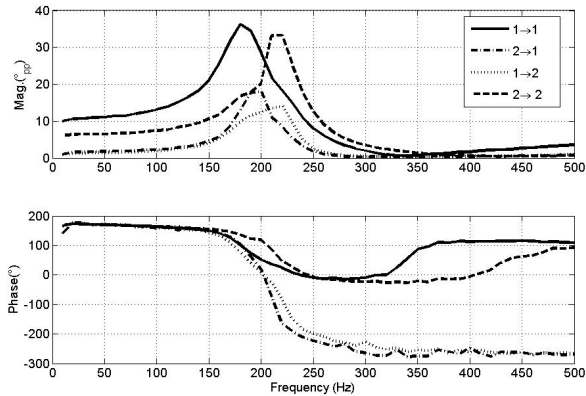


Fig. 8. Frequency response of a one wing structure mounted on a stiff plastic base to eliminate dynamics other than from the structure itself.

## V. FOUR DOF FLY NEST DESIGN

Given the new fiberoptic position sensor, we next designed a method of using this technology to characterize the full 4 DOF MFI. The most notable problem in switching from the 2 DOF polyurethane base to the 4 DOF was properly constraining all 4 actuators and the entire fly itself to place the sensors close enough. It is easy to constrain the MFI; however, it is quite difficult to allow the airframe of the MFI to behave as it would in free flight (with all internal resonances and couplings) while still holding the actuator ground still so that the actuator position can be sensed.

### A. Actuator Ground Design

For the 2 DOF test structure discussed in the previous section, the actuators were constrained with epoxy on the separate polyurethane bases shown in Fig. 6. However, on the 4 DOF MFI, the actuators need to be mounted parallel and very near each other but must not couple displacements to one another. This design constraint means that the actuator mount must not only resist bending due to point loads at the tips of the actuators, but also that the mount must resist torsional moments wanting to twist the base. Experimentally, using several layers of carbon fiber and attaching the four actuators to this rectangle, it has been found that resistance to this torsional moment is the most demanding design consideration.

It is known that the shape that resists torsion the best for a given cross sectional area of material is a cylinder.

However, it is very difficult to construct a cylinder from planar carbon fiber at this scale. We chose instead to mold the actuators in a 2 mm diameter cylinder made from polyurethane, in this case BJB Enterprises TC-781. Since weight is a concern, this particular polyurethane was chosen because when cured in normal air (i.e. not a vacuum as is recommended), the catalyst of the plastic foams with moisture in the air to introduce air pockets in the plastic matrix. Milled glass fibers were also mixed with the plastic when curing; by the rule of mixtures, this increases the torsional modulus of the material. The final polyurethane cylinder mount weighs approximately 10 mg.

The advantages of molding the actuators in a stiff, light plastic are obvious; the actuators need not be glued (they are molded in the plastic matrix) and wiring is now easier, for small holes can be carved in the plastic down to the actuator and filled with conductive epoxy to create an externally accessible wire terminal. A picture of the polyurethane cylinder with actuators and carbon fiber planks embedded appears in Fig. 13.

### B. Hardpoint Design

One other advantage of the polyurethane cylinder is that we can now mold a hardpoint in the plastic cylinder along with the actuators to clamp the entire MFI. As one can see from Fig. 1, the actuators in the cylindrical base on the MFI are internally contained in the structure. The actuators are obviously not externally accessible for the sensor as were the actuators used on the 2 DOF base. However, the sensor heads are small enough that they can rest in the space between each fourbar and actuator (separated by the slider crank) if the top and bottom of the MFI are exposed, as shown in Fig. 9.

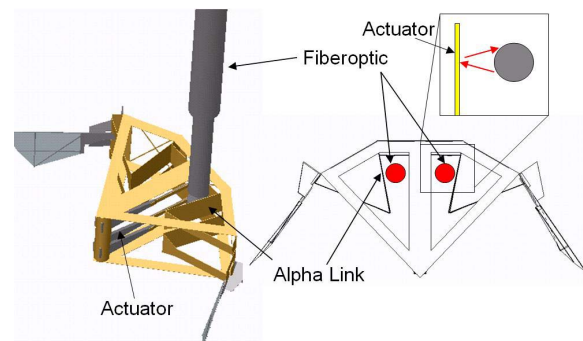


Fig. 9. Fiberoptic sensor alignment geometry for 4DOF MFI nest

The challenge here is to leave the top and bottom of the MFI open while grounding the actuator polyurethane base properly. We first tried to attach a multilayer carbon fiber hardpoint with epoxy to the plastic cylindrical base. The hardpoint could then be clamped with a standard 1 inch C-clamp which was embedded into glass reinforced polyurethane on the test stand. The remaining test stand pieces shown in Figure 10 are to align and restrain the fiberoptic sensors relative to the clamped fly.

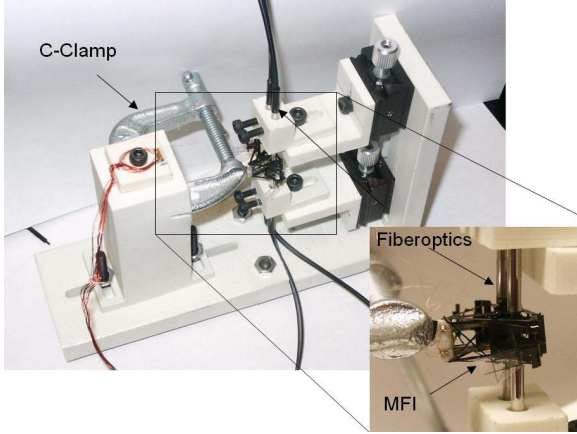


Fig. 10. 4DOF clamping and sensing test stand

However, the epoxy attaching the hardpoint to the cylindrical base was not nearly stiff enough and allowed the MFI as a whole to move drastically while characterization was attempted. The solution to this motion caused by inertial forces is to embed the hardpoint in the plastic cylindrical base that the actuators are also embedded in. This eliminates the glue attachment point resonance, but a resonance introduced by the hardpoint itself could still be a problem.

### C. Nest Frequency Response Testing

In order to properly characterize the MFI, the test stand must not introduce any resonances below the frequencies of interest in driving and controlling the MFI. Intuitively, this means all connections must be very stiff. The clamp provides a very strong connection to ground for the hardpoint; however, the hardpoint introduces a finite stiffness connection to the entire fly, and the fly will have a simple resonant mode as the hardpoint functions as a cantilever (see Fig. 11). If a lumped mass model of the fly is used (and neglecting more complicated internal resonances of the airframe), we can use a simple spring mass model of the system to find the dominant resonance. Considering the airframe as an infinitely stiff spring leading to the center of mass and applying a force here (as shown in Fig. 12), the stiffness of this beam is calculated by

$$y_{total} = \frac{FL^3}{3EI} + \frac{ML^2}{2EI} + L_{COM} \sin\left(\frac{ML}{EI} + \frac{FL^2}{2EI}\right) \quad (1)$$

The first term is the deflection of the hardpoint due to a force on the center of mass of the fly. The second term is due to the moment induced by a force on a fly and the lever arm of  $L_{COM}$ . The final term is due to the slope at the end of the hardpoint resulting in a displacement of the center of mass of the fly. Solving for  $F/y_{total}$  in this equation knowing  $M = F * L_{COM}$  and using the small angle approximation, one finds

$$k_{eff} = \frac{F}{y_{total}} \quad (2)$$

$$= \left( \frac{L^3}{3EI} + \frac{L_{COM}L^2}{2EI} + \frac{L_{COM}L^2 + 2L_{COM}^2L}{2EI} \right)^{-1} \quad (3)$$

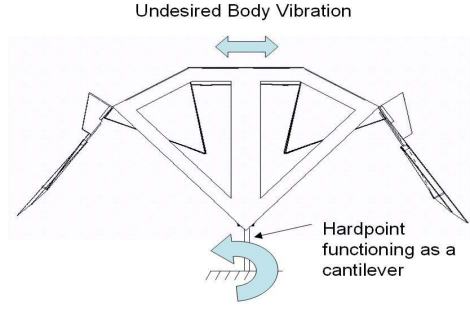


Fig. 11. Diagram of predictable but undesirable body vibrational mode

Knowing  $E_{CF} = 350GPa$ ,  $L_{COM} = 6.6mm$  and experimentally measuring  $L = 0.5mm$ , one finds that for two layers of carbon fiber ( $80 \mu m$ ), the resonant frequency of the clamped fly with hardpoint is predicted to be

$$f = \frac{1}{2\pi} \sqrt{\frac{k_{eff}}{m_{lumped}}} = 634Hz \quad (4)$$

This is only marginally acceptable, for drive frequencies with components at approximately 500 Hz are being considered. However, if one more layer of carbon fiber is used ( $h = 120 \mu m$ ), then the resonant frequency is predicted to be 1166 Hz. This frequency is safely higher than drive frequencies of interest, so three layers of carbon fiber were chosen for hardpoint construction.

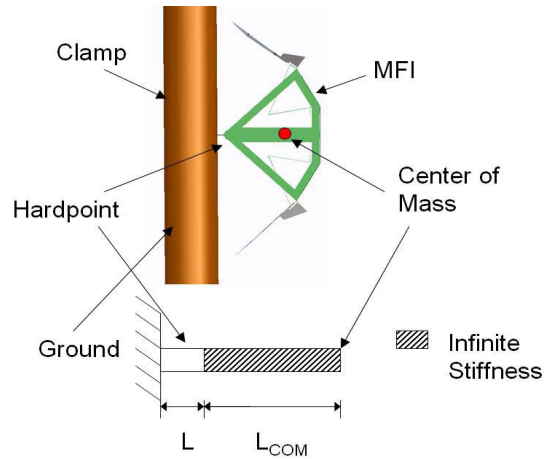


Fig. 12. Diagram of clamping mechanism and associated variables for resonance calculation

To experimentally verify the clamp mechanism without introducing added complexity by including possibly airframe internal resonances, the actuator core of the MFI consisting of the polyurethane cylinder base containing one actuator (along with three carbon fiber planks for stand-ins for the other actuators) and a hardpoint was constructed and is shown in Fig. 13. The one live actuator was driven

all the way to its resonance (around 3000 Hz) and the displacement of the actuator itself plus the displacements of the planks were measured with the custom fiberoptic sensors, looking for unwanted resonances. The setup is functionally similar to a full MFI in the clamp, except since the mass is lower, we brought the resonant frequency back into a measurable range by using only two layers of carbon fiber for the hardpoint.

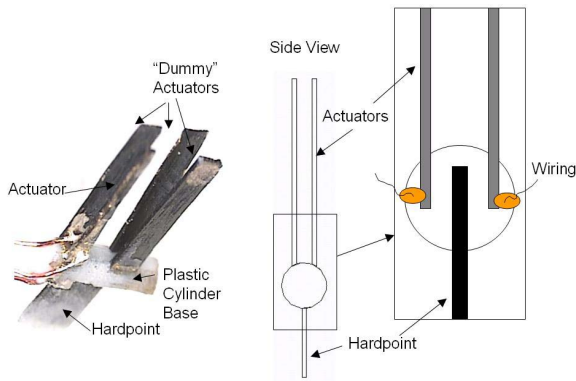


Fig. 13. Actuator and three carbon fiber beams embedded in polyurethane mount (gold paint at ends)

The predicted resonance of this mass at the end of the  $80\mu\text{m}$  hardpoint given by equations 3 and 4 is 1448 Hz. Fig. 14 is a magnitude Bode plot of the actuator and a Bode plot of two of the plank sensor signals, showing vibration of the entire structure as predicted. The resonant frequency for the entire structure was experimentally determined to be 1380 Hz, which is very close to the predicted 1448 Hz.

Finally, the full 4 DOF MFI was clamped in the nest and a single wing was characterized and compared to the results from the single wing shown in Fig. 8. The results of this test, which includes possible airframe compliances and resonances, appear in Fig. 15. As one can see, the Bode plots are quite similar to those presented earlier from the plastic base mounted structure. Differences in the frequency responses of the two systems can be explained through both airframe compliances and simple deviation in the construction of the two different systems.

## VI. CONCLUSION

Sensing the state of microrobots such as the MFI is a difficult task. We have presented an optical reflective sensing technology utilizing fiberoptics and associated circuitry that results in a sufficiently low profile sensing method. The sensor system is accurate to within  $5\mu\text{m}$  of motion and has a bandwidth of 3700 Hz. In combination with our experimentally verified hardpoint clamping technique, we can now characterize and control the 2 wing, 4 DOF MFI. Future work includes eliminating internal airframe resonances coupling the wings together in an undesirable way and finally reproducing the aerodynamic lift numbers presented previously in [6] on the two wing version of the MFI to achieve takeoff.

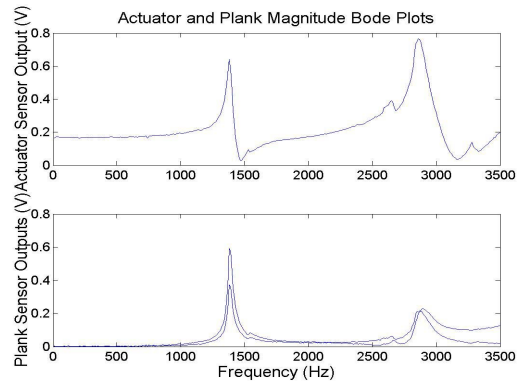


Fig. 14. Magnitude Bode plots for the actuator and two of the CF plank stand-ins

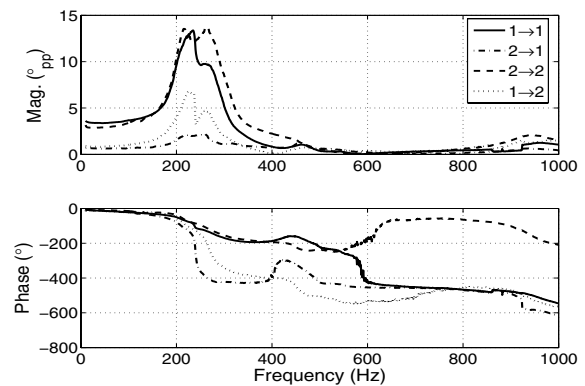


Fig. 15. Frequency response of one wing mounted on an entire 4 DOF MFI

## VII. ACKNOWLEDGMENTS

The authors would like to thank Dr. Richard Groff and Ranjana Sahai for insightful discussions and suggestions in the areas of sensing and mechanics.

## REFERENCES

- [1] Michael H. Dickinson, Fritz-Olaf Lehmann, and Sanjay P. Sane. Wing rotation and the aerodynamic basis of insect flight. *Science*, 284:1954–1960, June 18 1999.
- [2] R.S. Fearing, K.H. Chiang, M. Dickinson, D.L. Pick, M. Sitti, and J. Yan. Wing transmission for a micromechanical flying insect. In *IEEE International Conference on Robotics and Automation*, San Francisco, CA, 2000.
- [3] R.J. Wood, S. Avadhanula, M. Menon., and R.S. Fearing. Microrobotics using composite materials: The micromechanical flying insect thorax. In *IEEE International Conference on Robotics and Automation*, pages 1842–1849, Taiwan, 2003.
- [4] R.J. Wood and R.S. Fearing. Flight force measurements for a micromechanical flying insect. In *IEEE International Conference on Intelligent Robots and Systems*, Maui, 2001.
- [5] Domenico Campolo, Ranjana Sahai, and Ronald S. Fearing. Development of piezoelectric bending actuators with embedded piezoelectric sensors for micromechanical flapping mechanisms. In *IEEE International Conference on Robotics and Automation*, pages 3339–3346, Taiwan, 2003.
- [6] S. Avadhanula, R.J. Wood, E. Steltz, J. Yan, and R.S. Fearing. Lift force improvements for the micromechanical flying insect. In *International Conference on Intelligent Robots and Systems*, pages 1350–1356, Las Vegas, October 2003.